Observation of Pure-Spin-Current Diodelike Effect at the Au/Pt Interface

Pavlo Omelchenko,[1,*] Eric Arturo Montoya,[2] Erol Girt,[1] and Bret Heinrich[1]
[1]Department of Physics, Simon Fraser University, 8888 University Drive, Burnaby, British Columbia V5A 1S6, Canada
[2]Department of Physics and Astronomy, University of California, Irvine, California 92697, USA

(Received 15 October 2020; revised 31 May 2021; accepted 19 August 2021; published 24 September 2021)

Asymmetric charge transport at the interface of two materials with dissimilar electrical properties, such as metal-semiconductor and *p-n* junctions, is the fundamental feature behind modern diode and transistor technology. Spin pumping from a ferromagnet into an adjacent nonmagnetic material is a powerful technique to generate pure-spin currents, wherein spin transport is unaccompanied by net charge transport. It is therefore interesting to study pure-spin transport at the interface of two materials with different spin transport properties. Here we demonstrate asymmetric transport of pure-spin currents across an interface of dissimilar nonmagnetic materials Au/Pt. We exploit Py/Au/Pt/Co structures where spin pumping can generate pure-spin current from either Py or Co independently. We find that the transmission of pure-spin current from Au into Pt is twice as efficient as transmission from Pt into Au. Experimental results are interpreted by extending conventional spin-pumping, spin-diffusion theory to include boundary conditions of reflected and transmitted spin current at the Au/Pt interface that are proportional to the established spin chemical potentials on either side of the interface.

DOI: 10.1103/PhysRevLett.127.137201

Utilizing pure-spin current to manipulate the magnetic moment of a ferromagnet (FM) allows for transport of information without associated joule heating. A powerful technique to generate pure-spin current (hereinafter referred to as spin current) and investigate its transport properties within various materials is spin pumping. The effects of spin pumping were first detected by increases in magnetic damping of single ultrathin FM films in direct proximity to nonmagnetic metals (NMs) [1,2]. These early works showed that the damping enhancement was an interface effect, being inversely proportional to the thickness of the FM. The role of spin-orbit interaction was highlighted by Heinrich *et al.* [1].

Spin pumping was first demonstrated to be a nonlocal effect in magnetic heterostructures with two FMs in FM1-NM-FM2, where a resonantly driven FM1 acted as a spin pump and FM2 acted as a spin sink [3]. The theoretical description of the spin-pumping mechanism was first described by Tserkovnyak *et al.* [4] in terms of scattering matrix theory and by Šimánek and Heinrich [5] in terms of time-retarded interlayer exchange coupling. The two approaches were shown to lead to the same result [5]. It was understood that spin pumping resulted in a spin accumulation inside the NM, which could then be transported by spin diffusion. Heinrich *et al.* [6] expanded on this idea by simultaneously driving both FM1 and FM2 into spin pumping, resulting in coherent exchange of spin currents between the two ferromagnets and therefore cancellation of the enhancement in damping. This Letter unequivocally demonstrates the most important feature of spin pumping and spin diffusion: the communication of magnetic information through a nonmagnetic metal.

Early spin-pumping studies focused on simple FM-NM structures, where changes in magnetic damping in ultrathin FMs were used to determine the efficiency of spin pumping at various FM-NM interfaces as governed by the (renormalized) spin mixing conductance ($\tilde{g}_{\uparrow\downarrow}$) $g_{\uparrow\downarrow}$ and the spin-diffusion length in the adjacent NM λ_{sd}. NMs with relatively low spin-orbit interaction were first studied (Ag [7,8], Au [8,9], Cu [10,11]), finding good agreement between experiment and theory [12]. These metals were found to have relatively large spin-diffusion lengths ($\lambda_{\mathrm{sd,Ag}} = 80$ nm, $\lambda_{\mathrm{sd,Au}} = 31$ nm) [8]. Since then, spin pumping and spin transport have been studied in a variety of materials; spin pumping driven by insulating ferrimagnets [13–15] and antiferromagnets [16] and spin pumping into nonmetallic materials such as antiferromagnetic insulators [17–19] and organic semiconductors [20,21] have been demonstrated.

Recently, attention has been devoted to studies of spin transport in heavy metals with large spin-orbit interaction such as Pt, Ta, and W. Spin transport in these materials can be described by the conventional spin-diffusion model, but with a short spin-diffusion length ($\lambda_{\mathrm{sd}} \sim 1$–$3$ nm) [22–25]. Materials with large spin-orbit interaction are attractive as they allow charge-to-spin conversion effects and vice versa, such as spin Hall and inverse spin Hall effects [26]. These effects can be used for the all electrical generation or detection of spin currents. Electrical manipulation of the magnetization vector through spin-orbit torques is promising for the creation of practical spintronic devices, such as spin-orbit torque memory [27–29] and spin-orbit torque oscillators [30–33].

More recent studies of spin transport on FM-NM1-NM2 structures, where NM1 (Au, Cu) was a lower spin-orbit material than NM2 (Pd, Pt), have shown behavior that is outside the conventional spin-diffusion description. In such structures, oscillatory dependence of spin-pumping-induced damping on NM1 thickness was demonstrated [34,35]. Montoya *et al.* [34] attributed the oscillatory dependence in Fe/Au/Pd structure to quantum well states formed in the Au interlayer. They also explained the observed rapid decrease in spin-pumping-induced damping upon insertion of a thin Au layer to be due to a partial reflection of spin current at the Au/Pd interface [34] and not removal of proximity damping in Pd [36]. Additionally, it has be argued that spin-memory loss can impact pure-spin transport at such interfaces [37–40]. So far, however, spin pumping and spin transport have not been studied in such heterostructures with two ferromagnetic layers; here communication of spin currents between the ferromagnetic layers can be used to better determine bulk and interfacial spin absorption using spin-pump and spin-sink effects.

In this Letter, we study transport of spin current across the Au/Pt interface by spin pumping in three structures: Py/Au/Pt/Co, Py/Au/Pt, and Co/Pt, see Fig. 1. By exploiting directional spin-pump and spin-sink effects in the Py/Au/Pt/Co structure, we demonstrate a significantly larger reflection of pure-spin current coming from Pt at the Au/Pt interface than coming from Au. This asymmetry

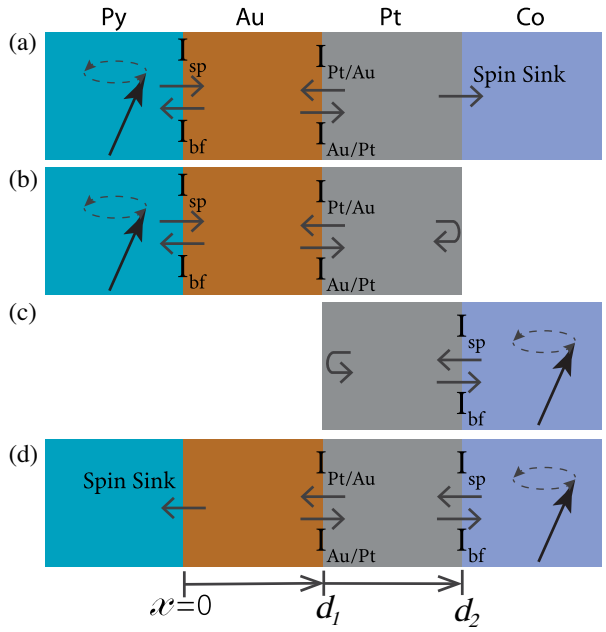

FIG. 1. Schematic of the studied structures $\overrightarrow{\text{Py}}$/Au/Pt/Co (a), Py/Au/Pt (b), Co/Pt (c) and Py/Au/Pt/$\overleftarrow{\text{Co}}$ (d), where the arrows indicate the ferromagnet put into precession. At the Au/Pt interface, a portion of the spin current is reflected and transmitted. At the other end of the structure, the spin current is either absorbed by the second ferromagnet (spin sink) or reflected at the metal-air boundary.

in pure-spin-current transport across the Au/Pt interface is analogous to the asymmetric charge transport in conventional diodelike devices; i.e., we demonstrate the discovery of a pure-spin-current diodelike effect. We show that all the data can be self-consistently described by assuming a combination of reflected and transmitted spin currents across Au/Pt proportional to the spin potential on either side of the interface.

The studied magnetic multilayer structures, Ta(3)/Py(6)/Au(3)/Pt(d_{Pt}), Ta(3)/Co(6)/Pt(d_{Pt}), and Ta(3)/Py(6)/Au(3)/Pt(d_{Pt})|Co(6)/Ta(3) were deposited on oxidized Si wafers by means of rf magnetron sputter deposition at room temperature. Here Py = $Ni_{80}Fe_{20}$, d_{Pt} is the Pt thickness, and the numbers in parentheses are thicknesses in nanometers. Further details of multilayer sample growth can be found in the Supplemental Material [41], which includes Ref. [42]. Atomic force microscopy reveals a root-mean-square roughness of the films ≤ 1 Å, see Supplemental Material [41]. For brevity, we will refer to the three studied structures as Py/Au/Pt, Co/Pt, and Py/Au/Pt/Co in the rest of the discussion.

Spin transport was studied via changes in magnetic Gilbert-like damping detected by ferromagnetic resonance (FMR). In-plane FMR measurements were carried out in a field-swept, field-modulated setup in a frequency range of 6–28 GHz. The FMR signal was interpreted by an admixture of the in-phase and out-of-phase components of rf susceptibility [43,44]. Example FMR data are shown in the Supplemental Material [41], which includes Ref. [45].

Spin pumping is an interface phenomenon that generates spin current from a dynamic ferromagnet into the adjacent nonmagnetic material, given by [4,5]

$$\boldsymbol{I}_{\text{sp}} = \frac{\hbar}{4\pi}\tilde{g}_{\uparrow\downarrow}\boldsymbol{n}\times\frac{d\boldsymbol{n}}{dt}, \tag{1}$$

where $\boldsymbol{n}$ is a unit vector pointing in the direction of the magnetic moment of the ferromagnet. The reduced spin-mixing conductance $\tilde{g}_{\uparrow\downarrow}$ governs the efficiency of spin pumping and accounts for a diffusive FM-NM interface [12,46]. Spin pumping leads to a nonequilibrium chemical potential imbalance for the spins in the nonmagnetic metal $\boldsymbol{\mu}^s$ and results in an accumulated spin density at the FM-NM interface [12]. The transport of spin accumulation inside NM can be described by spin-diffusion theory [47] with a material-dependent spin-diffusion length λ_{sd}.

The net spin current flowing out of the ferromagnet is related to the enhancement in damping by

$$\alpha_{\text{sp}} = \frac{\gamma}{M_s d_{\text{FM}}}\left(\boldsymbol{I}_{\text{sp1}} - \frac{\tilde{g}_{\uparrow\downarrow}}{4\pi}\boldsymbol{\mu}_1^s\right)\Big|_{x=0}, \tag{2}$$

where γ is the gyromagnetic ratio of the ferromagnet given by $\gamma = g\mu_B/\hbar$ and g is the Landé g factor. The accumulated

density $\boldsymbol{\mu}_1^s$ is determined by spin transport in the adjacent material system, which is governed by the spin-diffusion parameters within materials (spin-diffusion length λ_{sd} and single spin resistivity $\rho^{\uparrow}$) and interfacial transport terms (spin-mixing conductances $\tilde{g}_{\uparrow\downarrow}$). Complete details of the model used are provided in the Supplemental Material [41].

Two of the systems studied in this Letter are the commonly studied single FM structures: Co/Pt [Fig. 1(c)] and Py/Au/Pt [Fig. 1(b)]. The third type of system, Py/Au/Pt/Co, is a double FM, double NM structure of the form FM1-NM1-NM2-FM2. In the Py/Au/Pt/Co structure, the spin pumping can be either generated from Py or Co (see Fig. 1), resulting in two completely different datasets from the same structure. For clarity, we will distinguish the two datasets as $\overrightarrow{\text{Py}}$/Au/Pt/Co and Py/Au/Pt/$\overleftarrow{\text{Co}}$, where the arrow indicates the ferromagnet put into precession and therefore the source of the spin current, see Figs. 1(a) and 1(d), respectively.

For complete interpretation of the data we require spin-pumping, spin-diffusion parameters of both Au and Pt. Spin-pumping into Au has been studied in great detail and shown to be well described by the conventional spin-pumping and spin-diffusion model [6,9,48] with $\lambda_{sd,Au} = 31$ nm [8]. The single spin resistivity of Au is taken to be $\rho_{Au}^{\uparrow} = 8\ \mu\Omega\,\text{cm}$ [49]. We determine $\tilde{g}_{\uparrow\downarrow,\text{Py/Au}} = 1.7 \times 10^{15}\ \text{cm}^{-2}$ from the difference in damping between the $\overrightarrow{\text{Py}}$/Au/Co and $\overrightarrow{\text{Py}}$/Au [first yellow and blue point on Fig. 2(a)] [48].

The four remaining parameters describing spin transport in Py/Au/Pt/Co ($\tilde{g}_{\uparrow\downarrow,\text{Pt/Co}}$, $\lambda_{sd,Pt}$, $\rho_{Pt}^{\uparrow}$, and $\tilde{g}_{\uparrow\downarrow,\text{Au/Pt}}$) are related to Pt and its interface with Co and Au. In order to have unique fitting parameters, it is important to simultaneously fit all datasets with the same fitting parameters [24]. In this Letter, the spin-sink structure is $\overrightarrow{\text{Py}}$/Au/Pt/Co. The 3 nm Au layer is sufficiently thick to prevent interlayer exchange coupling between Py and Co, which is mediated by proximity polarized Pt [50,51]. Spin current pumped from Py passes through Au and Pt and gets absorbed by the Co layer. Since the Au layer is much thinner than $\lambda_{sd,Au}$, spin transport is quasiballistic and the spin current is negligibly absorbed. The spin-pumping damping of Py in $\overrightarrow{\text{Py}}$/Au/Pt/Co decreases with increasing Pt thickness, see yellow points in Fig. 2(a). This is the expected dependence on d_{NM} in a FM1-NM-FM2 structure, where FM2 acts as a nearly perfect spin-sink, allowing the maximum transfer of angular momentum and thus largest increase in damping in FM1. NMs act as diffusive absorbers of spin currents, where increasing NM thickness leads to increased backscattering of spin current being reabsorbed by FM1, thus decreasing the damping enhancement in FM1. The spin-pumping damping of $\overrightarrow{\text{Py}}$/Au/Pt increases with increasing Pt thickness [see blue points in Fig. 2(a)], consistent with expected behavior for a single FM-NM structure [24].

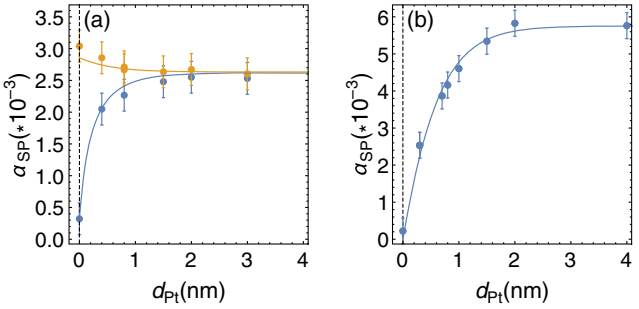

FIG. 2. Spin-pumping-induced damping data for (a) $\overrightarrow{\text{Py}}$/Au/Pt/Co (yellow), $\overrightarrow{\text{Py}}$/Au/Pt (blue), and (b) $\overrightarrow{\text{Co}}$/Pt structures as a function of Pt thickness d_{Pt}. The fits were done using conventional spin-pumping theory [12]. Solid lines represent simultaneous fits of the three datasets by Eq. (2) with conventional spin-pumping theory extended to include Au/Pt interface with boundary conditions of Eqs. (3) and (4).

In general the FM-NM and FM1-NM-FM2 structures are enough to uniquely determine the spin-transport parameters of single NM. However, in this Letter we aim to determine the effect of the Au/Pt interface on spin transport, where Pt has a much larger spin-orbit interaction. In view of this, we deposited Co/Pt structures to more accurately determine $\tilde{g}_{\uparrow\downarrow,\text{Pt/Co}}$, $\lambda_{sd,Pt}$, $\rho_{Pt}^{\uparrow}$ parameters. Figure 2(b) shows the magnetic damping of the Co/Pt rapidly approaches saturation with increasing Pt thickness for ~2 nm. This is consistent with $\lambda_{sd,Pt}$ observed in single crystal structures [52] and textured structures [51].

In contrast to the $\overrightarrow{\text{Py}}$/Au/Pt/Co data, the spin-pumping damping of Py/Au/Pt/$\overleftarrow{\text{Co}}$ (Fig. 3) does not have the typical NM dependence observed in FM1-NM-FM2 where FM1 is a spin-sink. In fact, the change in damping is very similar to $\overrightarrow{\text{Co}}$/Pt, see Fig. 2(b). This is very surprising considering that this structure has a spin sink (Py) on the other end, which one would expect to result in maximum damping for very thin d_{Pt} [51]. This observation suggests that the Au/Pt interface is preventing a large portion of the spin current from reaching the spin sink (Py). This behavior is not observed when spin pumping in the opposite direction ($\overrightarrow{\text{Py}}$/Au/Pt/Co), showing that the transport of pure-spin current across the Au/Pt interface is highly asymmetric.

To interpret these results, we present a new set of boundary conditions at the Au/Pt interface,

$$-\frac{\hbar}{2\rho_{Au}^{\uparrow}e^2}\frac{\partial\boldsymbol{\mu}_{Au}^s}{\partial x} = \frac{\tilde{g}_{\uparrow\downarrow,\text{Au/Pt}}}{4\pi}\boldsymbol{\mu}_{Au}^s - \frac{\tilde{g}_{\uparrow\downarrow,\text{Au/Pt}}}{4\pi}\boldsymbol{\mu}_{Pt}^s\Big|_{x=d_1}, \quad (3)$$

$$-\frac{\hbar}{2\rho_{Pt}^{\uparrow}e^2}\frac{\partial\boldsymbol{\mu}_{Pt}^s}{\partial x} = -\frac{\tilde{g}_{\uparrow\downarrow,\text{Au/Pt}}}{4\pi}\boldsymbol{\mu}_{Pt}^s + \frac{\tilde{g}_{\uparrow\downarrow,\text{Au/Pt}}}{4\pi}\boldsymbol{\mu}_{Au}^s\Big|_{x=d_1}. \quad (4)$$

Here, e is the fundamental charge and $\rho_{Au}^{\uparrow}(\rho_{Pt}^{\uparrow})$ is the single spin resistivity of Au(Pt). The efficiency of transfer of spin

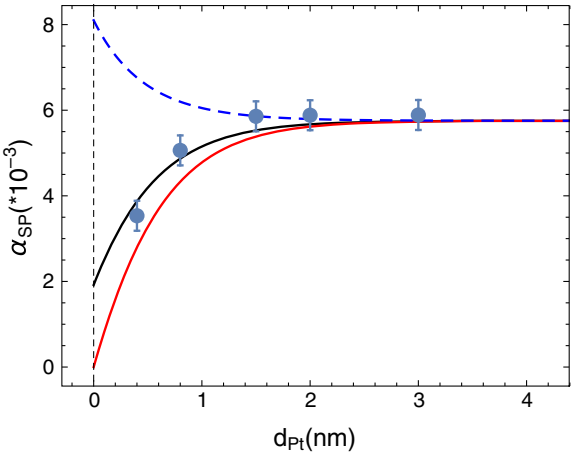

FIG. 3. Spin-pumping-induced damping in Co for Py/Au/Pt/$\overleftarrow{\text{Co}}$. The black line is a simulation with conventional spin-pumping theory extended to include Au/Pt interface with boundary conditions of Eqs. (3) and (4) and assuming fitting parameters as determined from Fig. 2. Simulated damping for Pt/$\overleftarrow{\text{Co}}$ (red line) and the spin-sink/Pt/$\overleftarrow{\text{Co}}$ (blue dashed line) are plotted assuming the same parameters as determined from the black line fit.

current from Au into Pt or from Pt into Au, $\tilde{g}_{\uparrow\downarrow,\text{Au/Pt}}$, is represented by a similar parameter as the spin-mixing conductivity at the interface FM-NM for spin pumping. These boundary conditions are akin to those at FM-NM, where the first term on the right-hand side represents the spin current injected from Au into Pt, and the second term on the right-hand side is the backflow from Pt into Au due to spin accumulation in Pt. Note, continuity of chemical potential [53] or continuity of spin accumulation [36] boundary conditions fail to represent the experimental data, see Supplemental Material [41].

Conceptually, the terms on the right-hand side of Eqs. (3) and (4) can be thought of as the forward spin current across Au/Pt (first term) and the spin current reflected at Au/Pt (second term). The left-hand side is the net spin current across the Au/Pt interface. The parameter $\tilde{g}_{\uparrow\downarrow,\text{Au/Pt}}$ characterizes the efficiency of spin transport across the Au/Pt interface. Including these boundary conditions in the conventional spin-pumping model, we simultaneously fit the $\overrightarrow{\text{Co}}$/Pt, $\overrightarrow{\text{Py}}$/Au/Pt, and $\overrightarrow{\text{Py}}$/Au/Pt/Co datasets shown in Fig. 2, resulting in $\tilde{g}_{\uparrow\downarrow,\text{Pt/Co}} = 7.6 \times 10^{15}$ cm^{-2}, $\lambda_{\text{sd,Pt}} = 1.0$ nm, $\rho_{\text{Pt}}^{\uparrow} = 61$ $\mu\Omega$ cm, and $\tilde{g}_{\uparrow\downarrow,\text{Au/Pt}} = 3.2 \times 10^{15}$ cm^{-2}. We note that $\tilde{g}_{\uparrow\downarrow,\text{Pt/Co}} = 7.6 \times 10^{15}$ cm^{-2} is large relative to other FM-NM interfaces (Fe/Au, Py/Ta, YIG/Pt, etc.); however, this is consistent with the literature where the typical range is $\tilde{g}_{\uparrow\downarrow,\text{Pt/Co}} \sim 4$–$9 \times 10^{15}$ cm^{-2} [37,54–56]. It has also been shown that the efficiency of spin pumping of Co can strongly depend on the interface [57]; however, in this Letter, both Py/Au/Pt/$\overleftarrow{\text{Co}}$ and $\overrightarrow{\text{Co}}$/Pt reach the same maximum damping, suggesting that both interfaces have similar $\tilde{g}_{\uparrow\downarrow,\text{Co/Pt}}$.

With all spin-transport parameters determined from the data presented in Fig. 2, the model is able to reproduce the unexpected thickness dependence of the Py/Au/Pt/$\overleftarrow{\text{Co}}$ dataset with no free parameters, see black line in Fig. 3. This thickness dependence is surprisingly very similar to $\overrightarrow{\text{Co}}$/Pt behavior, which we plot as the red line in Fig. 3. Importantly, in the limit of $d_{\text{Pt}} \overrightarrow{0}$, the model shows that the damping does not start at the intrinsic damping of Co ($d_{\text{Pt}} = 0$ of the red line) but at a slightly larger value, suggesting that some small portion of the spin current is passing through the Au/Pt interface and is being absorbed by the Py layer.

It is interesting to compare these results to the expected thickness dependence of a hypothetical spin-sink/Pt/$\overleftarrow{\text{Co}}$ structure assuming the same spin-transport parameters, see dashed blue line in Fig. 3. This suggests that the Au/Pt interface is playing a very large role in the observed spin transport. Note that the spin-sink/Pt/$\overleftarrow{\text{Co}}$ cannot be experimentally achieved since the spin sink (another ferromagnet) would magnetically couple through the Pt to the Co layer and would result in acoustic and optical precessional modes; this exact phenomenon was studied in our previous work [51].

The portion of reflected and forward spin currents at Au/Pt can be determined from Eqs. (3) and (4). The first term on the right-hand side of Eq. (3) is the forward spin current injected from Co due to spin pumping and impinging on the Au/Pt interface. The second term is effectively the spin current reflected at the Au/Pt interface and flowing back into Pt. The ratio of the chemical potentials at the interface ($\boldsymbol{\mu}_{\text{Pt}}^{s}/\boldsymbol{\mu}_{\text{Au}}^{s}$) is therefore the ratio of the forward to reflected spin currents, F_s/R_s. Using the spin-pumping parameters extracted from the fits and setting $d_{\text{Au}} = 3$ nm and $d_{\text{Pt}} = 1$ nm, we find that $F_s/R_s = 1.5$ for spin pumping from the Co in Py/Au/Pt/$\overleftarrow{\text{Co}}$. Note, if $F_s/R_s = 1$ then the forward current is perfectly compensated by the reflected spin current and the net flow across is zero. Therefore, $F_s/R_s - 1 = T_s/R_s$, where T_s is the net transmitted spin current. For the Py/Au/Pt/$\overleftarrow{\text{Co}}$ structure $F_s/R_s - 1 = 0.5$, implying that the reflected spin current is twice as large as the transmitted spin current. Normalizing the reflected and transmitted spin current by the forward spin current, one can show that only $T_s/F_s \sim 33\%$ of the spin current is transmitted, while $R_s/F_s \sim 67\%$ is reflected.

The spin-pumping data of the $\overrightarrow{\text{Py}}$/Au/Pt/Co and $\overrightarrow{\text{Py}}$/Au/Pt structures [Fig. 2(a)] does not show such a large reflection of spin current at the Au/Pt interface. The $\overrightarrow{\text{Py}}$/Au/Pt($d_{\text{Pt}} = 0$)/Co data point on Fig. 2(a) establishes the maximum spin pumping achievable in the $\overrightarrow{\text{Py}}$/Au/Co structure due to Co acting as a spin sink. Once again, we use the ratio of the chemical potentials at the Au/Pt interface ($\boldsymbol{\mu}_{\text{Au}}^{s}/\boldsymbol{\mu}_{\text{Pt}}^{s}$) to determine $F_s/R_s = 3.2$ for spin pumping from the Au side. Therefore, $F_s/R_s - 1 = 2.2$

for the $\overrightarrow{\mathrm{Py}}$/Au/Pt/Co structure, which implies that ~69% of the spin current is transmitted and ~31% is reflected.

Therefore, reflection at Au/Pt is much less when spin pumping from Py as compared to Co. However, there is still substantial reflection even when pumping from the Au side; this is consistent with experimental observations of quantum well states in the Fe/Au/Pd structures [34] and oscillatory spin polarization of Pt in Py/Cu/Pt structures [58], both of which suggest a reflection of pure-spin current at the Au/Pd or Cu/Pt interface. We note that our results are not well explained by spin-memory loss [37,40] or developing interface [59], as shown in the Supplemental Material [41], which includes Refs. [60,61].

Spintronic systems showing asymmetric charge transport have been previously demonstrated. One system is double-barrier magnetic tunnel junctions [62,63] that can behave similar to traditional diodes, where conductance can be asymmetric with respect to bias voltage polarity. Another system is based on semiconductor *p-n* bilayers that can be switched between insulating and conducting states by applied magnetic field [64,65]. Additionally, there is the spin-torque diode effect [66–68]; however, this effect is not due to asymmetric transport. Here a microwave ac current applied to a magnetoresistive device is rectified by dynamic magnetoresistance oscillations caused by spin torque and leads to a change in dc voltage across the device. In contrast, the effect demonstrated in this Letter results in an asymmetry in the transport of pure-spin currents where the net charge transport is zero.

In summary, we have experimentally studied pure-spin-current transport across the Au/Pt interface by means of spin pumping in Co/Pt, Py/Au/Pt and Py/Au/Pt/Co structures. Whereas the conventional diode effect is characterized by asymmetric charge transport, we find that the Au/Pt interface displays a diodelike effect with respect to pure-spin current; i.e., the spin transport is asymmetric at the Au/Pt interface. We find that the transmission of pure-spin current from Au into Pt is more than twice as efficient as transmission from Pt into Au. Our experimental results are well explained by extending conventional spin-pumping, spin-diffusion theory with boundary conditions for the spin chemical potential on either side of the Au/Pt interface. We anticipate this pure-spin-current diodelike effect can be utilized for enhanced tunability of the effective damping of magnetic layers in spintronics devices for applications such as spin-transfer torque–magnetic random-access memory [69–71], spin torque oscillators [72–74], and magnetic neuromorphic computing [75,76].

We would like to express our thanks to Natural Sciences and Engineering Research Council of Canada (NSERC) for its generous financial support without which this work would have not been possible.

*Corresponding author.
ppo@sfu.ca; Group website: http://surface-science.phys.sfu.ca.

[1] B. Heinrich, K. B. Urquhart, A. S. Arrott, J. F. Cochran, K. Myrtle, and S. T. Purcell, Phys. Rev. Lett. **59**, 1756 (1987).
[2] S. Mizukami, Y. Ando, and T. Miyazaki, Jpn. J. Appl. Phys. **40**, 580 (2001).
[3] R. Urban, G. Woltersdorf, and B. Heinrich, Phys. Rev. Lett. **87**, 217204 (2001).
[4] Y. Tserkovnyak, A. Brataas, and G. E. W. Bauer, Phys. Rev. Lett. **88**, 117601 (2002).
[5] E. Šimánek and B. Heinrich, Phys. Rev. B **67**, 144418 (2003).
[6] B. Heinrich, Y. Tserkovnyak, G. Woltersdorf, A. Brataas, R. Urban, and G. E. W. Bauer, Phys. Rev. Lett. **90**, 187601 (2003).
[7] B. Kardasz and B. Heinrich, Phys. Rev. B **81**, 094409 (2010).
[8] G. Woltersdorf, O. Mosendz, B. Heinrich, and C. H. Back, Phys. Rev. Lett. **99**, 246603 (2007).
[9] B. Kardasz, O. Mosendz, B. Heinrich, Z. Liu, and M. Freeman, J. Appl. Phys. **103**, 07C509 (2008).
[10] T. Gerrits, M. L. Schneider, and T. J. Silva, J. Appl. Phys. **99**, 023901 (2006).
[11] S. Mizukami, Y. Ando, and T. Miyazaki, Phys. Rev. B **66**, 104413 (2002).
[12] Y. Tserkovnyak, A. Brataas, G. E. W. Bauer, and B. I. Halperin, Rev. Mod. Phys. **77**, 1375 (2005).
[13] C. W. Sandweg, Y. Kajiwara, K. Ando, E. Saitoh, and B. Hillebrands, Appl. Phys. Lett. **97**, 252504 (2010).
[14] B. Heinrich, C. Burrowes, E. Montoya, B. Kardasz, E. Girt, Y.-Y. Song, Y. Sun, and M. Wu, Phys. Rev. Lett. **107**, 066604 (2011).
[15] A. Kapelrud and A. Brataas, Phys. Rev. Lett. **111**, 097602 (2013).
[16] P. Vaidya, S. A. Morley, J. van Tol, Y. Liu, R. Cheng, A. Brataas, D. Lederman, and E. del Barco, Science **368**, 160 (2020).
[17] H. Wang, C. Du, P. C. Hammel, and F. Yang, Phys. Rev. Lett. **113**, 097202 (2014).
[18] C. Hahn, G. de Loubens, V. V. Naletov, J. B. Youssef, O. Klein, and M. Viret, Europhys. Lett. **108**, 57005 (2014).
[19] T. Moriyama, S. Takei, M. Nagata, Y. Yoshimura, N. Matsuzaki, T. Terashima, Y. Tserkovnyak, and T. Ono, Appl. Phys. Lett. **106**, 162406 (2015).
[20] S. Watanabe, K. Ando, K. Kang, S. Mooser, Y. Vaynzof, H. Kurebayashi, E. Saitoh, and H. Sirringhaus, Nat. Phys. **10**, 308 (2014).
[21] D. Sun, K. J. van Schooten, M. Kavand, H. Malissa, C. Zhang, M. Groesbeck, C. Boehme, and Z. Valy Vardeny, Nat. Mater. **15**, 863 (2016).
[22] W. Zhang, V. Vlaminck, J. E. Pearson, R. Divan, S. D. Bader, and A. Hoffmann, Appl. Phys. Lett. **103**, 242414 (2013).
[23] C. T. Boone, J. M. Shaw, H. T. Nembach, and T. J. Silva, J. Appl. Phys. **117**, 223910 (2015).
[24] E. Montoya, P. Omelchenko, C. Coutts, N. R. Lee-Hone, R. Hübner, D. Broun, B. Heinrich, and E. Girt, Phys. Rev. B **94**, 054416 (2016).

[25] D. Jhajhria, N. Behera, D. K. Pandya, and S. Chaudhary, Phys. Rev. B **99**, 014430 (2019).

[26] J. Sinova, S. O. Valenzuela, J. Wunderlich, C. H. Back, and T. Jungwirth, Rev. Mod. Phys. **87**, 1213 (2015).

[27] I. M. Miron, K. Garello, G. Gaudin, P.-J. Zermatten, M. V. Costache, S. Auffret, S. Bandiera, B. Rodmacq, A. Schuhl, and P. Gambardella, Nature (London) **476**, 189 (2011).

[28] L. Liu, C.-F. Pai, Y. Li, H. W. Tseng, D. C. Ralph, and R. A. Buhrman, Science **336**, 555 (2012).

[29] S. Fukami, T. Anekawa, C. Zhang, and H. Ohno, Nat. Nanotechnol. **11**, 621 (2016).

[30] V. E. Demidov, S. Urazhdin, H. Ulrichs, V. Tiberkevich, A. Slavin, D. Baither, G. Schmitz, and S. O. Demokritov, Nat. Mater. **11**, 1028 (2012).

[31] Z. Duan, A. Smith, L. Yang, B. Youngblood, J. Lindner, V. E. Demidov, S. O. Demokritov, and I. N. Krivorotov, Nat. Commun. **5**, 5616 (2014).

[32] K. Wagner, A. Smith, T. Hache, J.-R. Chen, L. Yang, E. Montoya, K. Schultheiss, J. Lindner, J. Fassbender, I. Krivorotov *et al.*, Sci. Rep. **8**, 16040 (2018).

[33] J.-R. Chen, A. Smith, E. A. Montoya, J. G. Lu, and I. N. Krivorotov, Commun. Phys. **3**, 187 (2020).

[34] E. Montoya, B. Heinrich, and E. Girt, Phys. Rev. Lett. **113**, 136601 (2014).

[35] A. M. Gonçalves, F. Garcia, H. K. Lee, A. Smith, P. R. Soledade, C. A. C. Passos, M. Costa, N. M. Souza-Neto, I. N. Krivorotov, L. C. Sampaio, and I. Barsukov, Sci. Rep. **8**, 2318 (2018).

[36] E. Montoya, Spin pumping and spin transport in magnetic heterostructures, Ph.D. thesis, Simon Fraser University, 2016.

[37] J.-C. Rojas-Sánchez, N. Reyren, P. Laczkowski, W. Savero, J.-P. Attané, C. Deranlot, M. Jamet, J.-M. George, L. Vila, and H. Jaffrès, Phys. Rev. Lett. **112**, 106602 (2014).

[38] K. Chen and S. Zhang, Phys. Rev. Lett. **114**, 126602 (2015).

[39] X. Tao, Q. Liu, B. Miao, R. Yu, Z. Feng, L. Sun, B. You, J. Du, K. Chen, S. Zhang *et al.*, Sci. Adv. **4**, eaat1670 (2018).

[40] K. Gupta, R. J. H. Wesselink, R. Liu, Z. Yuan, and P. J. Kelly, Phys. Rev. Lett. **124**, 087702 (2020).

[41] See Supplemental Material at http://link.aps.org/supplemental/10.1103/PhysRevLett.127.137201 for experimental data and attempts to fit the data by alternative models including spin-memory loss.

[42] P. Omelchenko, E. A. Montoya, C. Coutts, B. Heinrich, and E. Girt, Sci. Rep. **7**, 4861 (2017).

[43] Z. Celinski, K. Urquhart, and B. Heinrich, J. Magn. Magn. Mater. **166**, 6 (1997).

[44] E. Montoya, T. McKinnon, A. Zamani, E. Girt, and B. Heinrich, J. Magn. Magn. Mater. **356**, 12 (2014).

[45] *Ultrathin Magnetic Structures 3*, edited by B. Heinrich and J. A. C. B. Bland (Spinger-Verlag, Berlin, 2005).

[46] K. M. Schep, J. B. A. N. van Hoof, P. J. Kelly, G. E. W. Bauer, and J. E. Inglesfield, Phys. Rev. B **56**, 10805 (1997).

[47] M. Johnson and R. H. Silsbee, Phys. Rev. B **37**, 5312 (1988).

[48] E. Montoya, B. Kardasz, C. Burrowes, W. Huttema, E. Girt, and B. Heinrich, J. Appl. Phys. **111**, 07C512 (2012).

[49] M. Isasa, E. Villamor, L. E. Hueso, M. Gradhand, and F. Casanova, Phys. Rev. B **91**, 024402 (2015).

[50] P. Omelchenko, B. Heinrich, and E. Girt, Appl. Phys. Lett. **113**, 142401 (2018).

[51] P. Omelchenko, E. Girt, and B. Heinrich, Phys. Rev. B **100**, 144418 (2019).

[52] S. Keller, L. Mihalceanu, M. R. Schweizer, P. Lang, B. Heinz, M. Geilen, T. Brächer, P. Pirro, T. Meyer, A. Conca, D. Karfaridis, G. Vourlias, T. Kehagias, B. Hillebrands, and E. T. Papaioannou, New J. Phys. **20**, 053002 (2018).

[53] C. T. Boone, H. T. Nembach, J. M. Shaw, and T. J. Silva, J. Appl. Phys. **113**, 153906 (2013).

[54] W. Zhang, W. Han, X. Jiang, S.-H. Yang, and S. S. P. Parkin, Nat. Phys. **11**, 496 (2015).

[55] C.-F. Pai, Y. Ou, L. H. Vilela-Leão, D. C. Ralph, and R. A. Buhrman, Phys. Rev. B **92**, 064426 (2015).

[56] C. Swindells, A. T. Hindmarch, A. J. Gallant, and D. Atkinson, Phys. Rev. B **99**, 064406 (2019).

[57] M. Tokaç, S. A. Bunyaev, G. N. Kakazei, D. S. Schmool, D. Atkinson, and A. T. Hindmarch, Phys. Rev. Lett. **115**, 056601 (2015).

[58] A. M. Gonçalves, F. Garcia, H. K. Lee, A. Smith, P. R. Soledade, C. A. C. Passos, M. Costa, N. M. Souza-Neto, I. N. Krivorotov, L. C. Sampaio, and I. Barsukov, Sci. Rep. **8**, 2318 (2018).

[59] E. Barati, M. Cinal, D. M. Edwards, and A. Umerski, Phys. Rev. B **90**, 014420 (2014).

[60] S. Azzawi, A. Ganguly, M. Tokaç, R. M. Rowan-Robinson, J. Sinha, A. T. Hindmarch, A. Barman, and D. Atkinson, Phys. Rev. B **93**, 054402 (2016).

[61] J. Ketterson and L. Windmiller, Phys. Rev. B **2**, 4813 (1970).

[62] M. Chshiev, D. Stoeffler, A. Vedyayev, and K. Ounadjela, Europhys. Lett. **58**, 257 (2002).

[63] A. Iovan, S. Andersson, Y. G. Naidyuk, A. Vedyaev, B. Dieny, and V. Korenivski, Nano Lett. **8**, 805 (2008).

[64] S. Joo, T. Kim, S. H. Shin, J. Y. Lim, J. Hong, J. D. Song, J. Chang, H.-W. Lee, K. Rhie, S. H. Han *et al.*, Nature (London) **494**, 72 (2013).

[65] J. S. Friedman, E. R. Fadel, B. W. Wessels, D. Querlioz, and A. V. Sahakian, AIP Adv. **5**, 117102 (2015).

[66] A. A. Tulapurkar, Y. Suzuki, A. Fukushima, H. Kubota, H. Maehara, K. Tsunekawa, D. D. Djayaprawira, N. Watanabe, and S. Yuasa, Nature (London) **438**, 339 (2005).

[67] Y. Suzuki and H. Kubota, J. Phys. Soc. Jpn. **77**, 031002 (2008).

[68] B. Fang, M. Carpentieri, X. Hao, H. Jiang, J. A. Katine, I. N. Krivorotov, B. Ocker, J. Langer, K. L. Wang, B. Zhang *et al.*, Nat. Commun. **7**, 11259 (2016).

[69] A. D. Kent and D. C. Worledge, Nat. Nanotechnol. **10**, 187 (2015).

[70] *Introduction to Magnetic Random-Access Memory*, edited by B. Dieny, R. B. Goldfarb, and K.-J. Lee, IEEE Magnetics (IEEE Press, Piscataway, NJ, 2017).

[71] E. A. Montoya, J.-R. Chen, R. Ngelale, H. K. Lee, H.-W. Tseng, L. Wan, E. Yang, P. Braganca, O. Boyraz, N. Bagherzadeh *et al.*, Sci. Rep. **10**, 10220 (2020).

[72] T. Chen, R. K. Dumas, A. Eklund, P. K. Muduli, A. Houshang, A. A. Awad, P. Dürrenfeld, B. G. Malm, A. Rusu, and J. Åkerman, Proc. IEEE **104**, 1919 (2016).
[73] C. Safranski, E. A. Montoya, and I. N. Krivorotov, Nat. Nanotechnol. **14**, 27 (2019).
[74] R. Lebrun, S. Tsunegi, P. Bortolotti, H. Kubota, A. S. Jenkins, M. Romera, K. Yakushiji, A. Fukushima, J. Grollier, S. Yuasa *et al.*, Nat. Commun. **8**, 15825 (2017).
[75] J. Grollier, D. Querlioz, K. Y. Camsari, K. Everschor-Sitte, S. Fukami, and M. D. Stiles, Nat. Electron Rev. **3**, 360 (2020).
[76] R. Matsumoto, S. Lequeux, H. Imamura, and J. Grollier, Phys. Rev. Applied **11**, 044093 (2019).